The EMBO Journal Vol.18 No.18 pp.4981–4987, 1999

High resolution AFM topographs of the *Escherichia coli* water channel aquaporin Z

Simon Scheuring, Philippe Ringler, Mario Borgnia[1], Henning Stahlberg, Daniel J.Müller, Peter Agre[1] and Andreas Engel[2]

M.E.Müller Institute for Structural Biology at the Biozentrum, University of Basel, Basel CH-4056, Switzerland and [1]Department of Biological Chemistry, Johns Hopkins University School of Medicine, 725 N. Wolfe Street, Baltimore, MD 21205, USA

[2]Corresponding author
e-mail: aengel@ubaclu.unibas.ch

Aquaporins form a large family of membrane channels involved in osmoregulation. Electron crystallography has shown monomers to consist of six membrane spanning α-helices confirming sequence based predictions. Surface exposed loops are the least conserved regions, allowing differentiation of aquaporins. Atomic force microscopy was used to image the surface of aquaporin Z, the water channel of *Escherichia coli*. Recombinant protein with an N-terminal fragment including 10 histidines was isolated as a tetramer by Ni-affinity chromatography, and reconstituted into two-dimensional crystals with $p42_12$ symmetry. Small crystalline areas with $p4$ symmetry were found as well. Imaging both crystal types before and after cleavage of the N-termini allowed the cytoplasmic surface to be identified; a drastic change of the cytoplasmic surface accompanied proteolytic cleavage, while the extracellular surface morphology did not change. Flexibility mapping and volume calculations identified the longest loop at the extracellular surface. This loop exhibited a reversible force-induced conformational change.

Keywords: atomic force microscopy/bacterial water channel/loops/sidedness/volume

Introduction

Aquaporins are ubiquitous membrane channels in bacteria, fungi, plants and animals. They are highly specific for water or small uncharged hydrophilic solutes and are involved in osmoregulation. Hydropathy analysis of the first sequenced members of this family indicated six membrane spans and two unusually long loops (Gorin *et al.*, 1984; Preston and Agre, 1991). Meanwhile, >160 genes have been sequenced, almost all having the highly conserved NPA motifs within these loops (Heymann and Engel, 1999). The role of the unique triplets remains to be established. Approximately half of these channel proteins are exclusively water selective and do not allow the permeation of small or charged solutes. Other channels facilitate the passage of small hydrophilic molecules such as glycerol or urea (Ishibashi *et al.*, 1997). Passage of ions through water channel proteins have been reported, and recent data suggest this to be regulated by pH (Yasui *et al.*, 1999).

The best characterized water channel is aquaporin-1 (AQP1) from human red blood cells (Agre *et al.*, 1993). Three-dimensional (3D) density maps of this protein have been established to a resolution of 6 Å by three groups (Cheng *et al.*, 1997; Li *et al.*, 1997; Walz *et al.*, 1997). These maps show a bundle of six highly tilted transmembrane helices that surround a central density formed by the long loops. These results confirm the hourglass model of Jung *et al.* (1994), who proposed a frame of six α-helices that houses the two NPA motif-carrying loops which fold back into the membrane to form a highly specific channel. The water flow per channel was found to be the same in two-dimensional (2D) crystals of AQP1 as in erythrocyte ghosts: 3×10^9 water molecules per channel per second (Zeidel *et al.*, 1992; Walz *et al.*, 1994b).

In *Escherichia coli*, a water channel has been identified by homology cloning (Calamita *et al.*, 1995). Sequence analysis of this bacterial channel, AqpZ, revealed a significant homology to AQP1. Recombinant AqpZ bearing a histidine tag has been produced and shown to be active (Borgnia *et al.*, 1999). 2D crystals with sizes ranging up to 5 μm have been assembled from this recombinant AqpZ tetramer by dialysis of a protein/lipid/detergent mixture (Ringler *et al.*, 1999). The 3D map of negatively stained preparations revealed the same packing arrangement as in AQP1 2D crystals, $p42_12$, while the 8 Å projection map from vitrified unstained preparations showed a striking similarity to the AQP1 and the major intrinsic protein (MIP) projection maps (Walz *et al.*, 1995; Hasler *et al.*, 1998; Ringler *et al.*, 1999).

We have used an atomic force microscope (AFM) (Binnig *et al.*, 1986) to measure the surface topography of AqpZ crystals in a native environment. As previously reported, this method allows protein surfaces to be imaged at subnanometer resolution (Müller *et al.*, 1995b; Schabert *et al.*, 1995; Mou *et al.*, 1996; Scheuring *et al.*, 1999). Topographs of AqpZ crystals bearing an N-terminal polyhistidine tag to allow rapid isolation exhibited a floppy protrusion related to the N-terminus that could be eliminated by proteolysis. This allowed the sidedness of AqpZ to be identified. After cleavage of the histidine tag, topographs had a lateral resolution of 7 Å and a vertical resolution of 1 Å. The surface topography could be related to the loops predicted from the sequence by hydropathy analysis.

Results

In the presence of 25 mM $MgCl_2$, the 2D crystals of AqpZ adsorbed to mica without wrinkles and were thus suitable for high-resolution imaging. To this end, the adsorption buffer was exchanged with the recording buffer

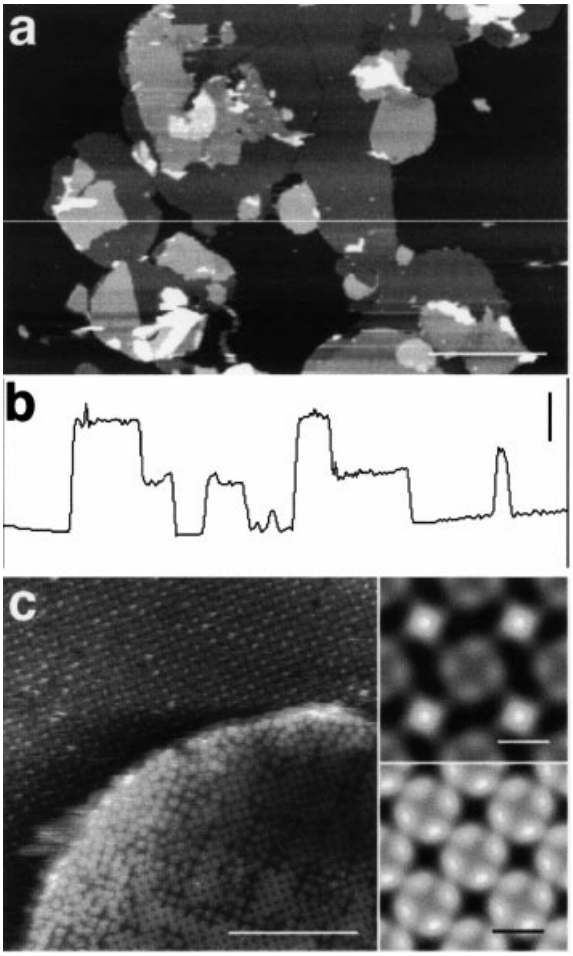

Fig. 1. (**a**) AFM topograph of AqpZ 2D crystals adsorbed to mica (recorded in buffer solution: 17 mM Tris–HCl pH 7.2, 150 mM KCl). Double and multi-layered areas can clearly be distinguished from single layer crystals by their higher appearance (scale bar, 2 μm; full gray scale, 30 nm). (**b**) Section analysis along the white line in image (a). The 2D crystals show a uniform height of 57 ± 4 Å (n = 45). Double layered areas appear as plateaus twice as high as the single layered crystal sheets (vertical scale bar, 50 Å). (**c**) AFM topograph of reconstituted AqpZ (recorded in buffer solution: 17 mM Tris–HCl pH 7.2, 150 mM KCl). A densely packed vesicle containing crystalline areas with $p4$ symmetry adsorbed onto a crystal sheet with $p42_12$ symmetry (scale bar, 100 nm; full gray scale, 20 nm). Top inset: average of the sheet with $p42_12$ symmetry (scale bar, 50 Å). Bottom inset: average of the crystalline areas with $p4$ symmetry within the densely packed vesicle (scale bar, 50 Å).

that was adjusted to electrostatically balance the van der Waals forces (Müller *et al.*, 1999a). The overview in Figure 1a demonstrates the flatness of the 2D crystals whose thickness was found to be 57 ± 4 Å (n = 45; Figure 1b).

At higher magnification the square lattice became distinct (Figure 1c, main frame, top). The unit cell dimensions were $a = b = 95 \pm 2$ Å, in excellent agreement with results from electron microscopy (Ringler *et al.*, 1999). Correlation averaging revealed a unit cell housing two tetramers in opposite orientations with respect to the membrane plane ($p42_12$ packing; Figure 1c, top right). The high signal-to-noise ratio of the AFM also allowed high resolution imaging on densely packed vesicles which only exhibited small crystalline areas comprising ~30 tetramers arranged with $p4$ symmetry (Figure 1c, main frame, bottom) The $p4$ crystals had unit cell dimensions of $a = b = 72 \pm 2$ Å and housed a single tetramer (Figure 1c, bottom right).

The recombinant AqpZ crystallized has an N-terminal fragment of 26 amino acids, containing a trypsin cleavage site at Arg26 and a His_{10} tag at amino acid positions 2–12 (Figure 2a; Borgnia *et al.*, 1999). As a consequence, a total of 104 amino acids, including 40 histidines, protruded from the cytoplasmic side of each tetramer. These peptides produced a strong signal in the AFM, resulting in a 20 ± 2 Å high peak (Figures 1c and 3a), the exact position and appearance of which depended critically on the force applied to the stylus, the scan speed and the direction of the scan (compare Figures 1c and 3a). This extreme flexibility prevented the resolution of substructure. To prove that the large protrusion observed indeed arose from the N-terminal domain, crystals were treated with trypsin (see Materials and methods) to cleave off this flexible end domain as documented in Figure 2b. The digested crystals exhibited a striking change; instead of an ill-defined protrusion of 20 Å height, the cytoplasmic side now showed four distinct protrusions each with a height of 3.5 ± 0.4 Å above the lipid bilayer (Figure 3b). In contrast, the extracellular side was not changed in either shape or height by the trypsin treatment (Figure 3c; see Table I). The extracellular side was not sensitive to trypsin digestion; however, it underwent a reversible conformational change when the force applied to the tip was increased during imaging. At minimal force (~80 pN) each AqpZ subunit showed three major protrusions probably related to the loops connecting the membrane spanning helices on the extracellular side (Figure 4a and c). Recording a second image of the same areas with a force increased by +80 pN, a drastic conformational change was observed (compare Figure 4a with b, and c with d). The extracellular AqpZ surface reversibly changed its rather circular appearance into a left-handed windmill which still protruded out of the membrane by 7 Å (Figure 4e). This force-induced conformational change was not influenced by the trypsin treatment, as illustrated by comparing the topographs of digested (Figure 4c and d) and undigested AqpZ crystals (Figure 4a and b). The digested cytoplasmic surface did not show the same force dependence, the minor force-induced conformational change was barely noticeable (Figure 4c and d, insets). The standard deviation (SD) map of 289 densely packed single tetramers (such as shown in Figure 4a) recorded at minimal force was calculated to identify the flexible regions of the extracellular surface (Müller *et al.*, 1998). As displayed in Figure 4f, one region exhibited a pronounced SD, while the rest yielded highly reproducible heights (SD ⩽0.2 Å). Interestingly, this flexible region also exhibited the major force-induced conformational change (compare left and right tetramer in Figure 4f).

Sequence based structure prediction postulates AqpZ to be a protein consisting of six transmembrane helices connected by three loops on the extracellular side and two loops on the cytoplasmic side, as well as two cytoplasmic termini (see Figure 2a). In agreement with this, on imaging at minimal force, three protrusions were found on the extracellular surface of the AqpZ monomer, one close to the 4-fold symmetry center, and one small and one elongated protrusion at the periphery (Figure 5a). Volume

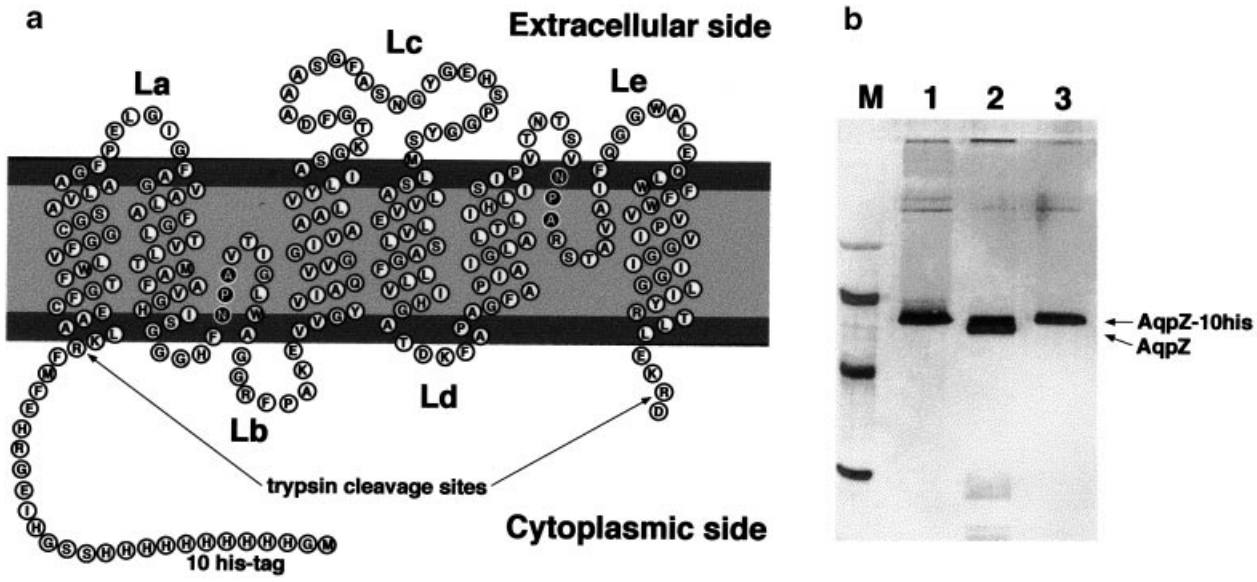

Fig. 2. (**a**) Amino acid sequence model of AqpZ showing the six membrane spanning helices derived from hydropathy analysis. Trypsin cleavage sites are located on Arg26 and Arg230. (**b**) Silver-stained SDS–polyacrylamide 10% (w/v) gel. Columns from left to right: (M) marker 97.4, 66.2, 42.7 and 31.0 kDa; (1) AqpZ solubilized in 2% OG. (2) AqpZ crystals after overnight trypsin treatment. The AqpZ band is broadened indicating that a minor part of the protein remained undigested. The two diffuse bands in the low molecular weight region (<30 kDa) correspond to trypsin and the cleaved N-terminal fragments. (3) AqpZ–10his crystals. The faint bands at high molecular weight (~200 kDa) in all three lanes arise from specific aggregates.

calculations (see Materials and methods) on the protrusion close to the 4-fold symmetry center resulted in 1278 ± 150 Å^3. The small peripheral protrusion yielded a volume of 984 ± 134 Å^3, while the elongated protrusion had a volume of 3187 ± 528 Å^3, the larger SD reflecting the flexibility of this region. The single protrusion observed per monomer on the digested cytoplasmic surface had a volume of 1222 ± 144 Å^3 (Figure 5b). Since the termini are removed (Figure 2a and b), this protrusion is expected to house loops B and D.

Discussion

Significant progress in the understanding of imaging conditions and the interpretation of topographs recorded with the AFM has allowed the surface topography of bacteriorhodopsin to be correlated with the helix-connecting loops to a lateral resolution of 5 Å (Müller *et al.*, 1999b). Here we have used this technology to study the surface of AqpZ, the first bacterial water channel identified (Calamita *et al.*, 1995). Its overexpression, isolation and 2D crystallization have recently been described (Borgnia *et al.*, 1999; Ringler *et al.*, 1999).

2D crystals adsorbed firmly and without folds or wrinkles to freshly cleaved mica in a high ionic strength buffer (Müller *et al.*, 1997). Subsequent change to a buffer adjusted to compensate for van der Waals interactions allowed their height to be measured accurately (Müller and Engel, 1997). The result, 57 ± 4 Å, compares favorably with the height previously reported for AQP1, 58 ± 3 Å (Walz *et al.*, 1996).

The $p42_12$ crystals of AqpZ with unit cell dimensions of $a = b = 95 \pm 2$ Å have similar lattice parameters to those found for AQP1 (unit cell dimensions: 96 ± 2 Å) (Walz *et al.*, 1996). However, the *p*4 crystals of AqpZ (unit cell dimensions of $a = b = 72 \pm 2$ Å) are more loosely packed than 2D crystals of MIP which also exhibit *p*4 symmetry (unit cell dimensions: $a = b = 64 \pm 1$ Å; Hasler *et al.*, 1998). This suggests that more lipid molecules are interspersed between the AqpZ tetramers within the small crystalline areas in the densely packed vesicles than in the highly ordered MIP crystals.

In experiments with undigested AqpZ crystals the N-terminal tail of 26 amino acids prevented the visualization of substructures on the cytoplasmic surface. The four weakly ordered protruding peptides, each containing 10 histidines, have a total mass of ~12 kDa, and appeared to interact strongly with the silicon nitride tip. Consequently, the cytoplasmic surfaces exhibited peaks of ~20 Å height that were influenced by the scan direction (Figures 1c and 3a). In spite of these large protrusions, the intervening extracellular sides could be resolved as tetramers with a central hole and four major protrusions.

After trypsin treatment both the extracellular and cytoplasmic surfaces could be imaged at high resolution on $p42_12$ crystals (Figures 3b and 4c). Not only did the extracellular side show a consistent surface appearance before and after trypsin treatment (compare central particles in the insets of Figure 4a and c), but also its height over the lipid bilayer was not affected by the proteolytic cleavage (Table I). In contrast, only a small cytoplasmic protrusion remained after trypsin digestion; the surface appearance changed from a single large protrusion to a well-defined tetramer protruding by only 3.5 Å over the lipid bilayer (Figure 3c). Thus removal of the large flexible cytoplasmic domains by trypsin allowed the unambiguous assignment of the AqpZ sidedness. This elegant method will be useful to determine the sidedness of other recombinant membrane proteins with the AFM.

The visualization and identification of distinct loops on a protein surface with the AFM has been shown for bacteriorhodopsin (Müller *et al.*, 1995b, 1999b). The

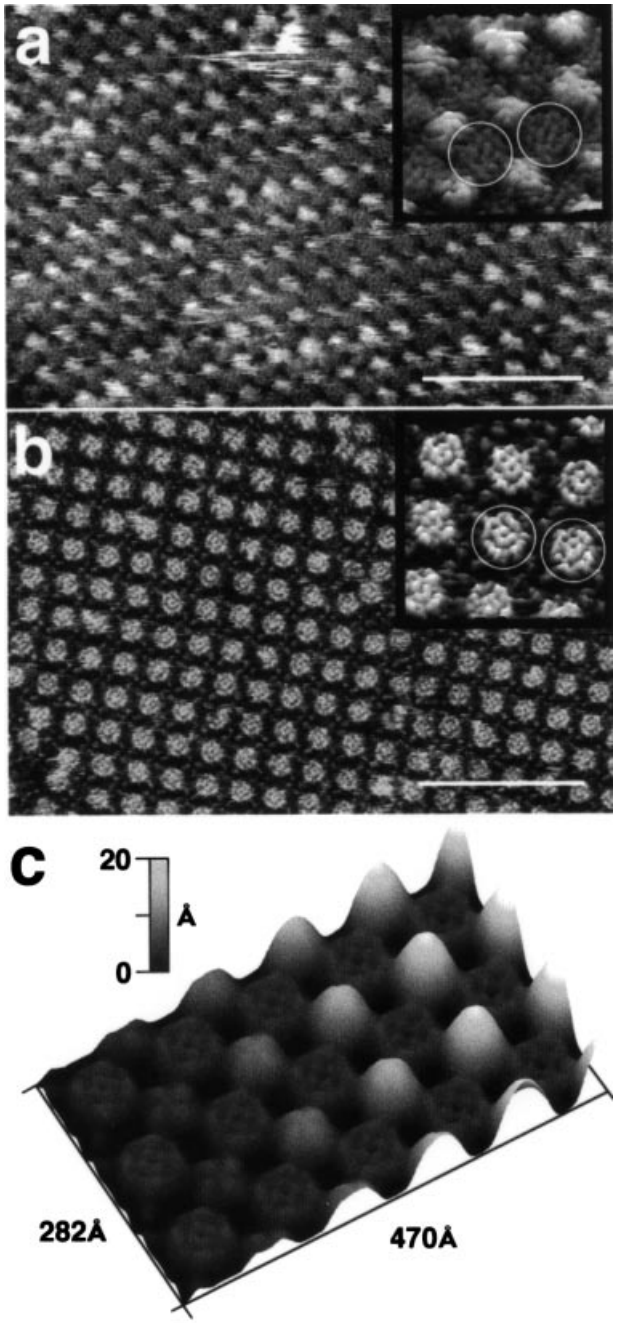

Fig. 3. (**a**) AFM topograph (recorded in buffer solution: 17 mM Tris–HCl pH 7.2, 150 mM KCl) of an AqpZ–10His 2D crystal with $p42_12$ symmetry recorded using minimal force (scale bar, 500 Å; full gray scale, 30 Å). Inset: relief view (tilt, 85°) of a 300 Å square, raw data; extracellular surfaces are marked by circles. (**b**) AFM topograph (recorded in buffer solution: 17 mM Tris–HCl pH 7.2, 150 mM KCl) of an AqpZ 2D crystal with $p42_12$ symmetry after trypsin treatment recorded using minimal force (scale bar, 500 Å; full gray scale, 10 Å). Inset: relief view (tilt, 85°) of a 300 Å square, raw data; extracellular surfaces are marked by circles. (**c**) 3D reconstruction of the trypsin cleavage process (see Figure 2a) observed on the cytoplasmic surface. On digestion this surface changes shape and height drastically in the location of the N-terminal His tags (top right, undigested state; bottom left, digested state).

reliability of topographic data acquired has been documented by direct comparison with results from electron microscopy (Karrasch *et al.*, 1994) and X-ray crystallography (Schabert *et al.*, 1995). In addition, a force-induced reversible conformational change observed on the cytoplasmic surface of bacteriorhodopsin has indicated the location of the longest cytoplasmic loop (Müller *et al.*, 1995a). Finally, structural features having the strongest variability in the raw data are enhanced in SD maps allowing flexible regions of proteins to be identified (Müller *et al.*, 1998). All three methods were applied to assess the surface topography of AqpZ. First, we have identified two approximately equal, small protrusions (984 and 1278 $Å^3$), and one large, elongated protrusion (3187 $Å^3$) at the extracellular surface of AqpZ (Figure 5). Secondly, by applying an additional force of ~80 pN to the tip during scanning, the large protrusion was found to undergo a drastic conformational change (Figure 4). Because this change was completely reversible, the same area could be scanned many times, and the change monitored repeatedly. Thirdly, the SD map calculated from 289 AqpZ tetramers indicated that the large protrusion was the most flexible one (Figure 4). Taken together, this suggests that this large surface domain located at the periphery of the tetramer with a total volume of ~3200 $Å^3$ is related to loop C of AqpZ and predicted to comprise of 26 amino acids (3700 $Å^3$) (Figure 2a).

Table I. Heights (Å) of surface protrusions of AqpZ before and after trypsin treatment

	Undigested $p4$ crystal	Undigested $p42_12$ crystal	Digested $p42_12$ crystal
Extracellular protrusion	7.3 ± 0.9	6.7 ± 1.0	7.0 ± 0.9
Cytoplasmic protrusion	18.6 ± 1.8	20 ± 2.0	3.5 ± 0.4

In spite of the limitations related to the tip geometry, an estimate of the volume of contoured protrusions is possible (Fritzsche and Henderson, 1996; Schneider *et al.*, 1998). We have tested the algorithms used to delineate protrusions and calculate their volumes on surface topographs of bacteriorhodopsin (Müller *et al.*, 1999b) and porin (Schabert *et al.*, 1995; Müller and Engel, 1999), and found them to produce correct volumes within an experimental error of $<$20%. The volumes accordingly calculated for the AqpZ extracellular protrusions are close to those expected from the sequence-predicted loops, although the small loops A (predicted as six amino acids, 900 $Å^3$) and E (nine amino acids, 1300 $Å^3$) cannot be unambiguously assigned. However, the position of the two loops remaining on the cytoplasmic surface after digestion could be defined. Importantly, the unambiguous determination of sidedness achieved using the AFM together with digestion experiments, is essential for the interpretation of structural data obtained from AqpZ crystals by cryo-electron microscopy.

In conclusion, structural information on the surface-exposed loops of a membrane channel has been acquired with the AFM. These data are complementary to those obtained by electron crystallography, which provides mainly the 3D density map of the membrane-resident part of the protein. Because the AFM is operated under physiological conditions, function-related structural changes can be directly assessed (Müller and Engel, 1999). Such experiments will be relevant to study the recently discovered regulation of water channels by pH (see Engel *et al.*, 1999).

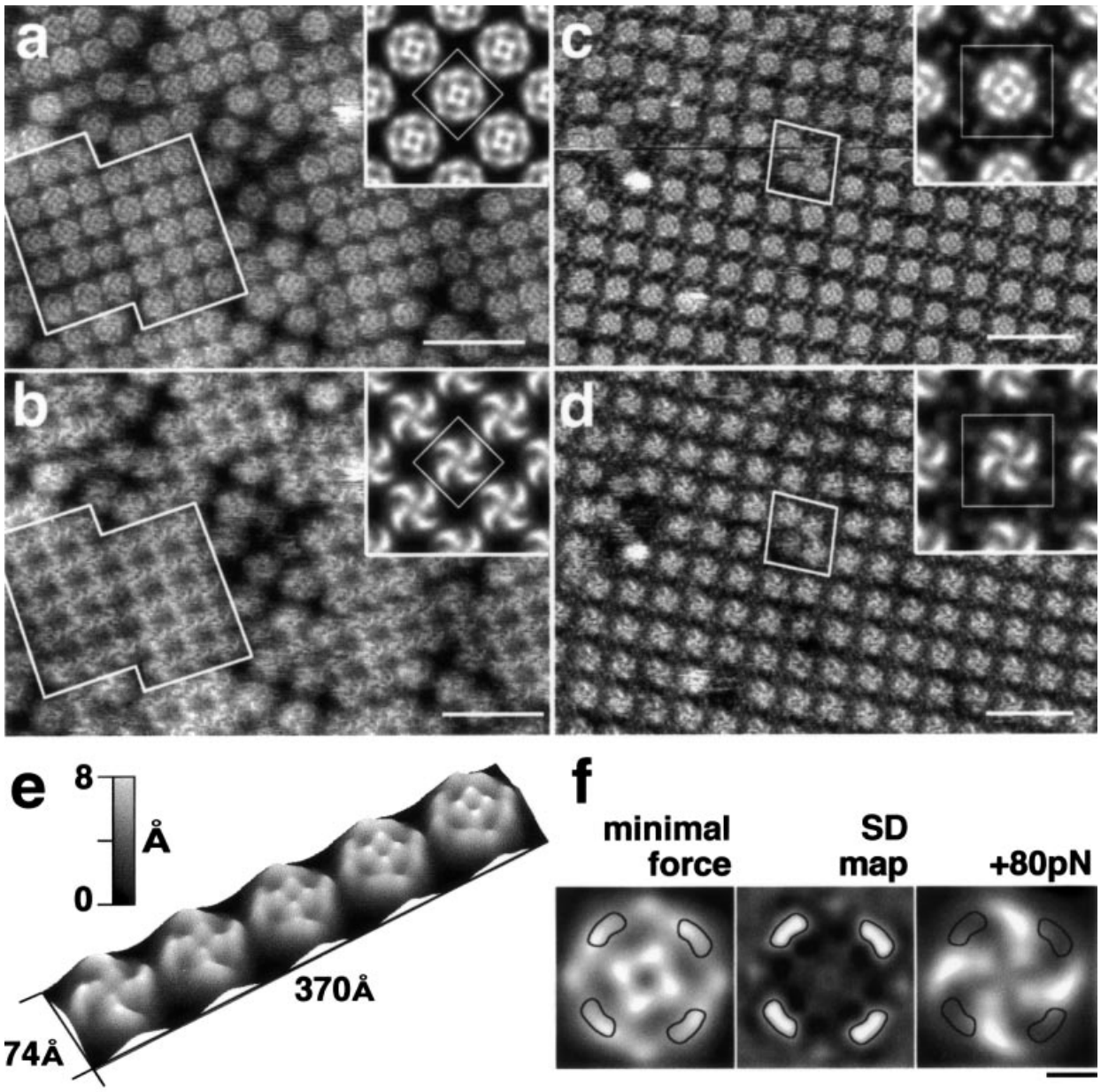

Fig. 4. (**a**) AFM topograph of AqpZ–His_{10} densely packed in a vesicle, scanned in buffer solution (17 mM Tris–HCl pH 7.2, 150 mM KCl) at minimal force (~80 pN) (scale bar, 250 Å; full gray scale, 18 Å). A small crystalline area with *p*4 symmetry is outlined. Inset: average of (a). The white square indicates the unit cell ($a = b = 72 \pm 2$ Å) which houses one tetramer. (**b**) AFM topograph of the same area as (a) recorded in buffer solution (17 mM Tris–HCl pH 7.2, 150 mM KCl) applying an additional force of +80 pN to the tip during scanning. The outlined area corresponds to the area marked in (a) (scale bar, 250 Å; full gray scale, 18 Å). Inset: average of (c). The white square indicates the unit cell ($a = b = 72 \pm 2$ Å) which houses one tetramer. (**c**) AFM topograph of trypsin treated AqpZ 2D crystals with $p42_12$ symmetry recorded in buffer solution (10 mM Tris–HCl pH 7.5, 150 mM KCl) using minimal force (~80 pN) (scale bar, 250 Å; full gray scale, 20 Å). The outlined area shows a pronounced lattice distortion. Inset: average of (c). The white square indicates the unit cell ($a = b = 95 \pm 2$ Å) which houses two tetramers. (**d**) AFM topograph of the same area as (c) recorded in buffer solution (10 mM Tris–HCl pH 7.5, 150 mM KCl) applying an additional force of +80 pN to the tip during scanning. Note the same lattice irregularity as in (c) (scale bar, 250 Å; full gray scale, 20 Å). Inset: average of (d). The white square indicates the unit cell ($a = b = 95 \pm 2$ Å) which houses two tetramers. (**e**) 3D reconstruction illustrating the effect observed on the extracellular surface when the imaging force is increased by +80 pN during scanning (top right, minimal force; bottom left, +80 pN). (**f**) Comparison of the averages of the extracellular surface at minimal force (left), the SD map (middle) and the extracellular surface average at a additional force of +80 pN (right) (full image sizes, 72 Å). The outlined regions in the middle image represent a SD of ~0.7 Å. These regions correspond to the four elongated peripheral protrusions in the minimal force average which are strongly displaced in the average gained from images recorded at +80 pN.

Materials and methods

Reconstitution

Large 2D crystals were produced by dialysis as described by Ringler *et al.* (1999). Recombinant AqpZ isolated by Ni-affinity chromatography (Borgnia *et al.*, 1999) was solubilized in 2% *n*-octyl-β-D-glucoside (OG) at a concentration of 0.5 mg/ml and mixed with dimyristoyl phosphatidyl choline/palmitoyl oleoyl phosphatidyl choline (DMPC/POPC) (1:1) solubilized in 2% OG to a final lipid-to-protein ratio of 0.3. The mixture was dialyzed against a detergent-free buffer (20 mM citric acid pH 6.0, 200 mM NaCl, 100 mM $MgCl_2$, 3 mM NaN_3, 10% glycerol) for 3 days. 2D crystals were washed by centrifugation and resuspended in adsorption buffer (see below).

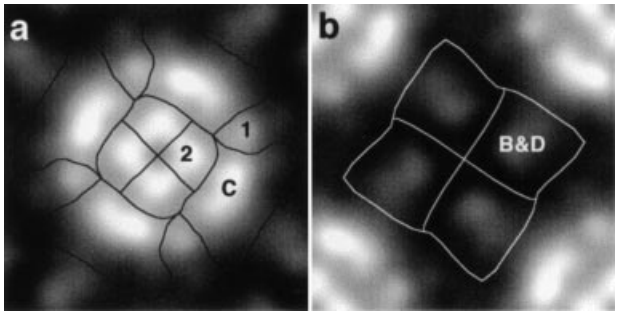

Fig. 5. Proposed assignment and borderlines between adjacent loops of the AqpZ tetramer. The *x*, *y* and *z* scalings used for 3D integration of the protruding volumes are derived from high resolution AFM topographs (full image sizes, 95 Å). (**a**) Extracellular surface exposing protrusions 1, 2 and C with volumes of 984 ± 134 Å^3, 1278 ± 150 Å^3 and 3187 ± 528 Å^3, respectively. Protrusions 1 and 2 correspond to loops A and E. The similarity of their volumes prevents an unambiguous assignment. (**b**) Cytoplasmic surface having only one defined protrusion housing loops B and D with a volume of 1222 ± 144 Å^3.

Trypsin digestion

For cleavage of the N-terminal fragment, AqpZ–His_{10} crystals were incubated overnight at 4°C with trypsin (1 mg/ml). The crystals were then washed twice through centrifugation in a table centrifuge (Heraeus Biofuge A) at 5000 r.p.m. for 3 min with subsequent removal of the supernatant and addition of fresh buffer solution. After trypsin treatment, samples were investigated by SDS–PAGE using 10% (w/v) acrylamide gels.

Atomic force microscopy

Mica prepared as described (Schabert and Engel, 1994) was used as support. For each experiment the mica was freshly cleaved with Scotch tape and imaged in 30–50 µl of adsorption buffer (10 mM Tris–HCl pH 7.5, 150 mM KCl, 25 mM $MgCl_2$) to check the cleavage quality; 3 µl of protein crystal solution (0.1 mg/ml) was then injected into the adsorption buffer drop on the mica surface. After 2 h the sample was carefully rinsed with recording buffer (10 mM Tris–HCl pH 7.5, 150 mM KCl), which was optimized to achieve high resolution as described (Müller *et al.*, 1999a). Imaging was performed with a commercial Nanoscope III AFM (from Digital Instruments, Santa Barbara, CA) equipped with a 120 µm scanner (J-scanner) and oxide-sharpened Si_3N_4 cantilevers with a length of 120 µm (k = 0.1 N/m) (from Olympus Ltd, Tokyo, Japan). The AFM was operated in contact mode applying constantly minimal forces (<0.2 nN) at a scan frequency of 4–6 Hz. The instrument was calibrated using layered crystals of $MoTe_2$ as described previously (Müller and Engel, 1997).

Image processing

AFM images of crystalline areas were processed by correlation averaging using the SEMPER image processing system (Saxton *et al.*, 1979). Tetramers of disordered regions were aligned and averaged by a single particle averaging protocol, and SD maps were calculated to assess the reproducibility of height measurements and to identify flexible regions (Müller *et al.*, 1998). To calculate the volumes of distinct protrusions in such an average, a SEMPER routine was used to determine the borderlines between adjacent elevations. To this end, a 3 × 3 pixel box was scanned over the image and all the central pixels having a lower gray value than any of the four pairs of adjacent pixels were identified as borderline. Outlined areas were evaluated by integrating all the pixels determined within this boundary using unit cell dimensions and heights determined with the AFM.

Acknowledgements

The authors would like to thank Dr S.A.Müller for proofreading and discussing the manuscript. We also thank D.Fotiadis and L.Hasler for inspiring discussions. The work was supported by the Maurice E.Müller foundation of Switzerland, the Swiss National Foundation for Scientific Research (grant 4036-44062 to A.E.), the Swiss Priority Project for Micro and Nano System Technology and the French INSERM (to P.R.).

References

Agre,P., Preston,G., Smith,B., Jung,J., Raina,S., Moon,C., Guggino,W. and Nielsen,S. (1993) Aquaporin CHIP: the archetypal molecular water channel. *Am. J. Physiol.*, **265**, F436–F476.

Binnig,G., Quate,C.F. and Gerber,C. (1986) Atomic force microscope. *Phys. Rev. Lett.*, **56**, 930–933.

Borgnia,M., Kozono,D., Calamita,G., Nielsen,S., Maloney,P.C. and Agre,P. (1999) Functional reconstitution and characterization of *E. coli* Aquaporin-Z. *J. Mol. Biol.*, in press.

Calamita,G., Bishai,W., Preston,G., Guggino,W. and Agre,P. (1995) Molecular cloning and characterization of AQPZ, a waterchannel from *Escherichia coli*. *J. Biol. Chem.*, **270**, 29063–29066.

Cheng,A., van Hoek,A.N., Yeager,M., Verkman,A.S. and Mitra,A.K. (1997) Three-dimensional organization of a human water channel. *Nature*, **387**, 627–630.

Engel,A., Fujiyoshi,Y. and Agre,P. (1999) The importance of aquaporin water channel protein structures. *EMBO J.*, **18**, in press.

Fritzsche,W. and Henderson,E. (1996) Volume determination of human metaphase chromosomes by scanning force microscopy. *Scan. Microsc.*, **10**, 103–108

Gorin,M.B., Yancey,S.B., Cline,J., Revel,J.-P. and Horwitz,J. (1984) The major intrinsic protein (MIP) of the bovine lens fiber membrane: Characterization and structure based on cDNA cloning. *Cell*, **39**, 49–59.

Hasler,L., Walz,T., Tittmann,P., Gross,H., Kistler,J. and Engel,A. (1998) Purified lens major intrinsic protein (MIP) forms highly ordered tetragonal two-dimensional arrays by reconstitution. *J. Mol. Biol.*, **297**, 855–864.

Heymann,J.B. and Engel,A. (1999) Aquaporins: phylogeny, structure and physiology of water channels. *News Physiol. Sci.*, in press.

Ishibashi,K., Kuwahara,M., Gu,Y., Kageyama,Y., Tohsaka,A., Suzuki,F., Maruma,F. and Sasaki,S. (1997) Cloning and functional expression of a new water channel abundantly expressed in the testis permeable to water, glycerol and urea. *J. Biol. Chem.*, **272**, 20782–20786.

Jung,J., Preston,G., Smith,B., Guggino,W. and Agre,P. (1994) Molecular structure of the water channel through aquaporin CHIP. The hourglass model. *J. Biol. Chem.*, **269**, 14648–14654.

Karrasch,S., Hegerl,R., Hoh,J.H., Baumeister,W. and Engel,A. (1994) Atomic force microscopy produces faithful high-resolution images of protein surfaces in an aqueous environment. *Proc. Natl Acad. Sci. USA*, **91**, 836–838.

Li,H., Lee,S. and Jap,B.K. (1997) Molecular design of aquaporin-1 water channel as revealed by electron crystallography. *Nature Struct. Biol.*, **4**, 263–265.

Mou,J., Czajkowsky,D.M., Sheng,S., Ho,R. and Shao,Z. (1996) High resolution surface structure of *E. coli* GroES oligomer by atomic force microscopy. *FEBS Lett.*, **381**, 161–164.

Müller,D.J. and Engel,A. (1997) The height of biomolecules measured with the atomic force microscope depends on electrostatic interactions. *Biophys. J.*, **73**, 1633–1644.

Müller,D.J. and Engel,A. (1999) pH and voltage induced structural changes of porin OmpF explain channel closure. *J. Mol. Biol.*, **285**, 1347–1351.

Müller,D.J., Büldt,G. and Engel,A. (1995a) Force-induced conformational change of bacteriorhodopsin. *J. Mol. Biol.*, **249**, 239–243.

Müller,D.J., Schabert,F.A., Büldt,G. and Engel,A. (1995b) Imaging purple membranes in aqueous solution at subnanometer resolution by atomic force microscopy. *Biophys. J.*, **68**, 1681–1686.

Müller,D.J., Amrein,M. and Engel,A. (1997) Adsorption of biological molecules to a solid support for scanning probe microscopy. *J. Struct. Biol.*, **119**, 172–188.

Müller,D.J., Fotiadis,D. and Engel,A. (1998) Mapping flexible protein domains at subnanometer resolution with the AFM. *FEBS Lett.*, **430**, 105–111.

Müller,D.J., Fotiadis,D., Scheuring,S., Müller,S.A. and Engel,A. (1999a) Electrostatically balanced subnanometer imaging of biological specimens by atomic force microscopy. *Biophys. J.*, **76**, 1101–1111.

Müller,D.J., Sass,H.-J., Mülller,S., Büldt,G. and Engel,A. (1999b) Surface structures of native bacteriorhodopsin depend on the molecular packing arrangement in the membrane. *J. Mol. Biol.*, **285**, 1903–1909.

Preston,G.M. and Agre,P. (1991) Isolation of the cDNA for erythrocyte integral membrane protein of 28 kilodaltons: Member of an ancient channel family. *Proc. Natl Acad. Sci. USA*, **88**, 11110–11114.

Ringler,P., Borgnia,M., Stahlberg,H., Agre,P. and Engel,A. (1999) Strucure of the water channel AqpZ from *Escherichia coli* revealed by electron crystallography. *J. Mol. Biol.*, in press.

Saxton,W.O., Pitt,T.J. and Horner,M. (1979) Digital image processing: Semper system. *Ultramicroscopy*, **4**, 343–354.
Schabert,F.A. and Engel,A. (1994) Reproducible acquisition of *Escherichia coli* porin surface topographs by atomic force microscopy. *Biophys. J.*, **67**, 2394–2403.
Schabert,F.A., Henn,C. and Engel,A. (1995) Native *Escherichia coli* OmpF porin surfaces probed by atomic force microscopy. *Science*, **268**, 92–94.
Scheuring,S., Müller,D.J., Ringler,P., Heymann,J.B. and Engel,A. (1999) Imaging streptavidin 2D crystals on biotinylated lipid monolayer at high resolution with the atomic force microscope. *J. Microsc.*, **193**, 28–35.
Schneider,S.W., Larmer,J., Henderson,R.M. and Oberleithner,H. (1998) Molecular weights of individual proteins correlate with molecular volumes measured by atomic force microscopy. *Pflügers Arch.*, **435**, 362–367.
Walz,T., Smith,B., Zeidel,M., Engel,A. and Agre,P. (1994) Biologically active two-dimensional crystals of aquaporin CHIP. *J. Biol. Chem.*, **269**, 1583–1586.
Walz,T., Typke,D., Smith,B.L., Agre,P. and Engel,A. (1995) Projection map of aquaporin-1 determined by electron crystallography. *Nature Struct. Biol.*, **2**, 730–732.
Walz,T., Tittmann,P., Fuchs,K.H., Müller,D.J., Smith,B.L., Agre,P., Gross,H. and Engel,A. (1996) Surface topographies at subnanometer resolution reveal asymmetry and sidedness of aquaporin-1. *J. Mol. Biol.*, **264**, 907–918.
Walz,T., Hirai,T., Murata,K., Heymann,J.B., Mitsuoka,A., Fujiyoshi,Y., Smith,B.L., Agre,P. and Engel,A. (1997) The 6Å three-dimensional structure of aquaporin-1. *Nature*, **387**, 624–627.
Yasui,M., Kwon,T.H., Knepper,M.A., Nielsen,S. and Agre,P. (1999) Aquaporin-6: An intracellular vesicle water channel protein in renal epithelia. *Proc. Natl Acad. Sci. USA*, **96**, 5808–5813.
Zeidel,M.L., Ambudkar,S.V., Smith,B.L. and Agre,P. (1992) Reconstitution of functional water channels in liposomes containing purified red cell CHIP28 protein. *Biochemistry*, **31**, 7436–7440.

Received June 1, 1999; revised July 19, 1999; accepted July 20, 1999